Materials Horizons

Communication

Solid-state-processing of δ-PVDF†

Jaime Martín[a], Dong Zhao[b] (赵冬), Thomas Lenz[b,c], Ilias Katsouras[d], Dago M. de Leeuw[b,e] and Natalie Stingelin[a,f]*

Received 00th January 20xx,
Accepted 00th January 20xx

DOI: 10.1039/x0xx00000x

www.rsc.org/

Poly(vinylidene fluoride) (PVDF) has long been regarded as an ideal piezoelectric 'plastic' because it exhibits a large piezoelectric response and a high thermal stability. However, the realization of piezoelectric PVDF elements has proven to be problematic, amongst others, due to the lack of industrially-scalable methods to process PVDF into the appropriate polar crystalline forms. Here, we show that fully piezoelectric PVDF films can be produced via a single-step process that exploits the fact that PVDF can be molded at temperatures below its melting temperature, i.e. via solid-state-processing. We demonstrate that we thereby produce δ-PVDF, the piezoelectric charge coefficient of which is comparable to that of biaxially stretched β-PVDF. We expect that the simplicity and scalability of solid-state processing combined with the excellent piezoelectric properties of our PVDF structures will provide new opportunities for this commodity polymer and will open a range of possibilities for future, large-scale, industrial production of plastic piezoelectric films.

Conceptual Insights

Here, we advance a solution for the the long-standing issue of producing 'plastic' piezoelectric items without the need to mechanical stretch thin foils — which so far has limited use of piezoelectric plastics to only a very few applications. More specifically, we show that a strategy frequently used for the processing of poly(tetra fluoroethylene) (PTFE; i.e. Teflon®) can be employed to produce piezoelectric structures in one single processing step with the commodity polymer poly(vinylidene fluoride) (PVDF) rather having to use the more complex and more expensive copolymers.

Introduction

Since the discovery in the 1970s that poly(vinylidene fluoride) (PVDF) [1, 2] can display a large piezoelectric response, this plastic has been the subject of intense research, and ubiquitous applications in everyday life have been foreseen, for instance, in sensing, energy harvesting, acoustics and information storage [3, 4, 5, 6, 7]. However, processing PVDF into a piezo-/ferroelectric form has proven to be challenging, amongst others due to the lack of industrially-scalable methods that can be applied for this purpose. The reason for this difficulty is that the ferro- and piezoelectricity of PVDF is linked to the coherent spatial distribution of the local C-F dipoles along the polymer backbone and its macromolecules' long-range packing order. Because of the variety of chain- and dipole arrangements that can be adopted, PVDF indeed exhibits at least four well-identified polymorphs, referred to as the α, β, γ and δ-phase [8, 9]. The α-phase is at ambient conditions the thermodynamically stable polymorph. Fig. 1a shows the projection of the chain arrangement in α-PVDF along the *c* axis of the unit cell. The orthorhombic, centrosymmetric unit cell contains two chains in tg^+tg^- conformation [10, 11]. Due to the anti-parallel packing of the chains in the unit cell, their dipole moments cancel out, rendering the α-phase non-polar and paraelectric. In contrast, the other PVDF

[a] Department of Materials and Centre of Plastic Electronics, Imperial College London, London SW7 2AZ, UK. E-mail: natalie.stingelin@mse.gatech.edu
[b] Max-Planck Institute for Polymer Research, Ackermannweg 10, 55128 Mainz, Germany
[c] Graduate School Materials Science in Mainz, Staudinger Weg 9, 55128 Mainz, Germany
[d] Holst Centre, High Tech Campus 31,5656AE Eindhoven, The Netherlands
[e] Faculty of Aerospace Engineering, Delft University of Technology, Kluyverweg 1, 2629 HS Delft, The Netherlands
[f] School of Materials Science and Engineering and School of Chemical & Biomolecular Engineering, Georgia Institute of Technology, 311 Ferst Drive, Atlanta, Georgia 30332, USA

† Electronic Supplementary Information (ESI) available: [details of any supplementary information available should be included here]. See DOI: 10.1039/x0xx00000x

polymorphs, *i.e.* the β-, γ- and δ-phases, are polar, hence ferroelectric and concomitantly piezoelectric [9]. The β-PVDF is the most pursued phase because it exhibits the highest ferroelectric and piezoelectric properties amongst the PVDF polymorphs — and of all polymers in general [2]. The orthorhombic unit cell has two chains in an all-*trans (ttt)* conformation [12] resulting in a net dipole moment per unit cell of 8 x 10^{-30} Cm [13]. Since PVDF is a semicrystalline polymer with a crystallinity of about 50%, it can be estimated that thin films made of this PVDF polymorph should feature a remanent polarization of around 9 μC cm^{-2}. The γ-phase of PVDF, which can be regarded as a mixture of the α- and β-phase, crystallizes in a monoclinic unit cell with four chains in a $t_3g^+t_3g^-$ conformation [14]. Therefore, the dipole moment is smaller than that of the β-phase. The third polar phase, the so-called δ-phase, is known since 1978 [9, 15, 16, 17, 18]. The crystal structure of this forgotten phase has recently been refined [5, 19]. The δ-phase is the polar version of the α-phase; both phases have the same lattice constants and chain conformation (tg^+tg^-) [15, 19]. However, in δ-PVDF, every second chain is rotated 180º around the chain axis (Fig. 1a). In order to prevent impossibly small interchain fluorine-fluorine distances, the macromolecules are shifted by half of the *c*-axis lattice constant. As a consequence, the remanent polarization, *i.e.* the displaced charge density at zero bias, amounts to 7 μC cm^{-2} and, thus, is comparable to that of β-PVDF.

Crystallization of PVDF from the melt or solution typically leads to the non-polar, paraelectric α-phase. Reported processing routes to obtain one of the polar PVDF phases are summarized in Fig. 1b. β-PVDF is commercially available, but it is produced in a two-step-process by biaxially stretching melt-processed α-PVDF, limiting the product range to free-standing foils. γ-PVDF is experimentally very challenging to access although recent work indicates that it can be formed in spatially confined systems [20, 21]. Finally, δ-PVDF has only been realized by applying high electric fields (≥ 170 MV/m) on α-PVDF structures. This process is called electroforming and it frequently results in the breakdown of both the electrode and the polymer [19] – an issue that has rendered δ-PVDF so far an impractical option from an industrial perspective.

Here, we present a simple route to produce piezoelectric δ-PVDF films allowing the assessment of the piezoelectric charge

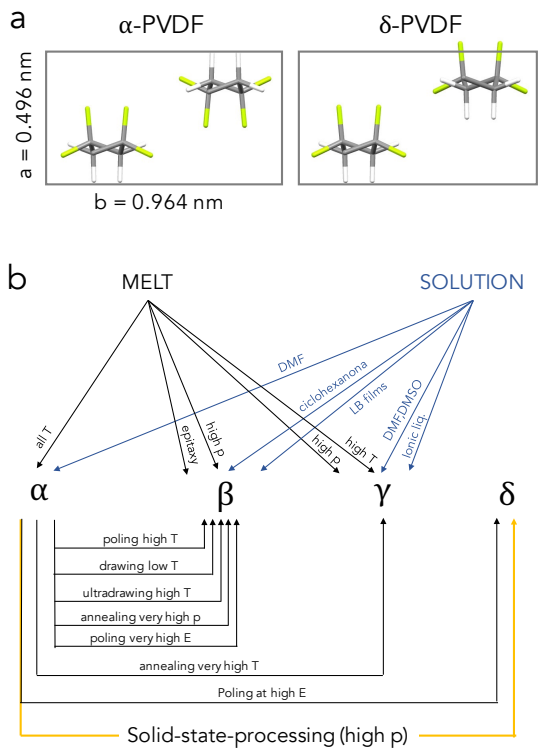

Fig. 1. Molecular arrangement and processing routes towards polar PVDF phases (adapted from [9]). a) Projections onto the *a-b* plane of the unit cell of the chain arrangement in, respectively, α- and δ-PVDF. (b) Processing routes of PVDF towards polar forms. δ-PVDF has been hitherto realized by applying high electric fields (≥ 170 MV/m) on α-PVDF, which frequently results in the breakdown of both the electrode and the polymer. Solid-state processing provides a simple, cost-efficient route to produce δ-PVDF films.

coefficient, d_{33}, of this PVDF polymorph for the first time after almost 40 years [16, 22]. Our method exploits the solid-state-processing of α-PVDF, *i.e.* the application of moderate pressures (~20 kN/cm^2) below the melting temperature, to induce a phase transition from the paraelectric α-PVDF phase to the polar δ-phase. Solid-state processing is already used, for instance, to manufacture products of poly(tetrafluoroethylene) (PTFE – better known as Teflon® [23]). The versatility of this process has recently been further highlighted by the successful fabrication of organic semiconducting films with high bulk charge-carrier mobility [24]. In the case of PVDF, solid-state processing is efficient and simple; indeed, it leads in one single step to δ-PVDF films – in contrast to the relatively elaborate mechanically stretching of α-PVDF films to produce foils of β-PVDF currently employed in industry.

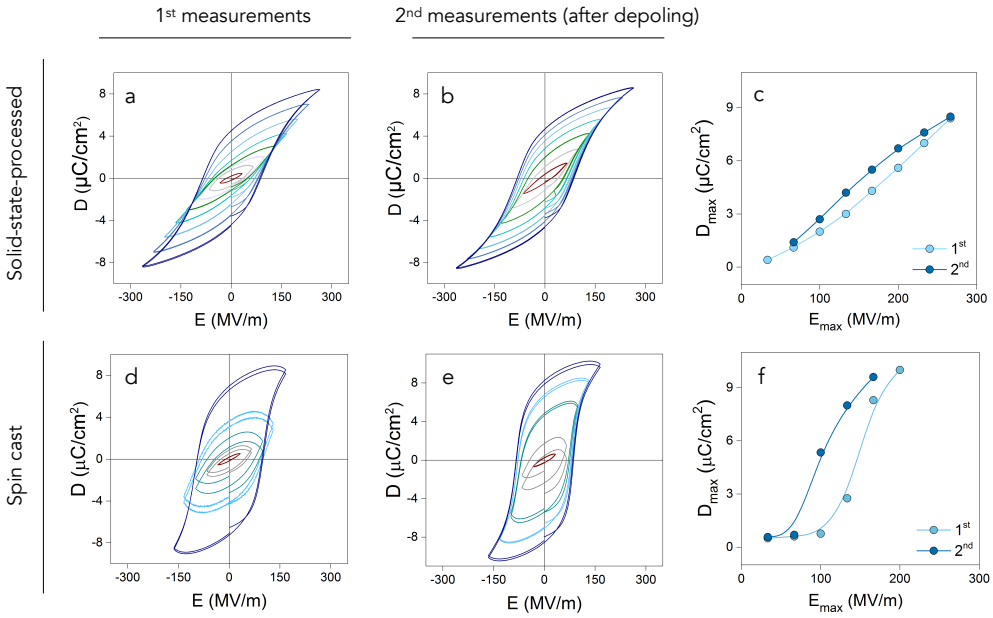

Figure 2. Ferroelectric behaviour and piezoelectric strain of solid-state pressed and spin-cast PVDF films. (a) Hysteresis loops of solid-state processed PVDF films measured with stepwise increasing electric field (amplitude). (b) Re-measured hysteresis loops after electrically depoling the film (a). (c) Maximum displacement as a function of electric field for a solid-state processed PVDF film as obtained from the first and second set of measurements. (d) Hysteresis loops of a spin-coated PVDF film measured with stepwise increasing electric field (amplitude) which shows that the initially prepared film is electroformed into a polar PVDF at high electric field. (e) Re-measured hysteresis loops after electroforming the spin-cast PVDF film. (f) Maximum displacement as a function of electric field for a spin-coated PVDF film as obtained from the first and second set of measurements.

Results and discussion

Films of PVDF were prepared by compression molding commercially purchased powder in a manual hot press at temperatures below the melting temperature of α-PVDF, *i.e.* at temperatures between 140 °C and 150 °C (ESI†). The pressure was thereby progressively increased up to ~20 kN/cm^2 and applied for 5 min. Subsequently, the films were cooled to ambient temperature under pressure. No coherent films could be produced when the pressing temperature was below 130 °C; and when pressing temperatures between 130 °C and 140 °C were used, films were obtained that were generally heavily cracked. In strong contrast, at higher pressing temperatures, the process led to highly transparent films of ~30 μm thickness and an area of about 1 cm^2 (Fig S1 ESI†).

In order to assess the ferroelectric properties of such solid-state pressed films (pressed at temperatures above 140 °C), we measured hysteresis loops after evaporating 30 nm Au electrodes on both sides of the free-standing structures (Fig. 2). Experimental details are provided in the ESI†. In the first set of measurements, with increasing amplitude of the applied electric field from 30 MV/m to 250 MV/m, the loops gradually open (Fig. 2a). The inner loops only slightly exceed the outer loops, which indicates that electroforming can be disregarded as a source of the ferroelectric response. We emphasize that the opening of the inner loops was gradual and not step-wise. The latter occurs in the case electroforming plays a role. We furthermore note that formation of "dead" interfacial layers either during metallization or due to fatigue can influence the hysteresis loops. In our measurements, we do not observe any imprint for this. Also, we had taken special care to avoid fatigue effects by adjusting the measurement protocol and by using pristine capacitors for each measurement. Excluding, thus, these extrinsic effects, we conclude that the as-prepared, solid-state films are ferroelectric, implying that this process directly induces a polar PVDF phase, which displays a coercive field, E_c, of 110 MV/m for the saturated loop, and a saturated polarization of 7 μC cm^{-2}.

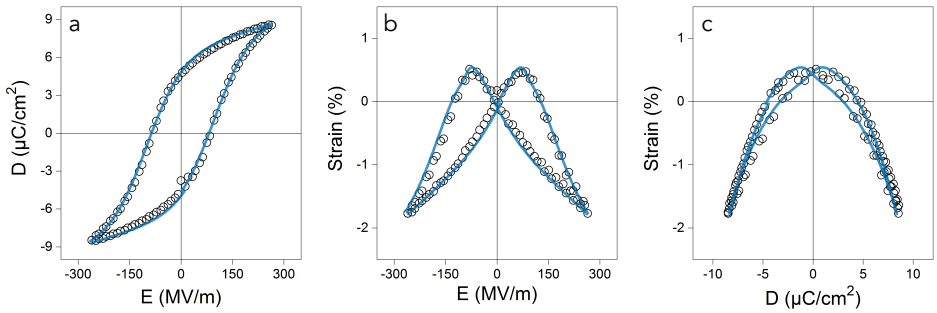

Fig. 3 Ferroelectric hysteresis and piezoelectric strain in solid-state pressed PVDF films. Measured (black) and modelled (blue) electric displacement curves (a) and strain (b), both measured vs. electric field. (c) Corresponding strain vs. electric displacement loops.

We repeated the hysteresis measurements after electrically depolarizing the solid-state pressed films with an alternating electric field of decreasing amplitude [5] — similar to the procedures used to demagnetize a ferromagnetic material [25]. We find that the second set of hysteresis loops (Fig. 2b) are similar to the loops obtained in the first measurements, which further supports our conclusion that solid-state processing directly leads to a polar ferroelectric PVDF form.

For comparison, we performed control measurements on free-standing, spin-cast PVDF films, which consist of the α-phase (Experimental details of the sample preparation are provided in the ESI†). The first set of measurements (Fig. 2d) show that at low electric fields, the loops resemble those obtained for a leaky capacitor. However, when the electric field exceeded 170 MV/m, the loops abruptly open, adopting a hysteretic shape typical for a ferroelectric material. This stepwise behavior indicates that at high electric field, spin-cast films are electroformed into a polar PVDF phase. In accord with this observation is the fact that the loops obtained in the second measurements (Fig. 2e) gradually open, resembling those of the solid-state pressed films.

The direct formation of polar PVDF upon hot pressing can further be highlighted by plotting the extracted values of the maximum value of the displacement as a function of electric field. Fig. 2c shows that for solid-state processed PVDF the values for the first and second measurement are very similar, establishing that polar PVDF was formed in one step during compression molding. In contrast, for spin-cast films the values for the first and the second set of measurements differ strongly (Fig. 2f). This stepwise increase of displacement with electric field implies that spin-coated PVDF is electroformed into polar PVDF, leading after electroforming to a relation between maximum displacement and electric field that is similar to that of solid-state processed polar PVDF.

Having established that a polar, piezoelectric PVDF phase is formed via solid-state processing, we measured simultaneously the electric displacement and strain of the solid-state pressed films. The displacement as a function of electric field is presented in Fig. 3a, and the strain as function of electric field and of displacement is presented in Fig. 3b,c. The strain can be quantitatively described by a model previously used to explain the negative piezoelectric effect. of PVDF and its copolymers [2]. The strain comprises the polarization-induced electrostrictive strain and an additional term resulting from the electro-mechanical coupling between the crystalline and amorphous fractions of PVDF. The displacement and strain can be simultaneously fitted as a function of electric field. Intriguingly, a perfect fit is obtained for the solid-state pressed PVDF films (Fig. 3). From the fit, we can extract a value of the piezoelectric charge coefficient, d_{33}, of -36 pm/V. Interestingly, this value is comparable to that of biaxially stretched β-PVDF (-31 pm/V), and it is slightly higher than that of electroformed δ-PVDF (respectively, -13 pm/V [16] and -15 pm/V [22]).

The question that remains to be answered is what polar PVDF phase is induced during the solid-state pressing process. To address this issue, we conducted wide-angle X-ray scattering (WAXS) measurements (ESI†). The WAXS patterns of as-received PVDF powder (light blue) and a solid-state pressed film (dark blue) are displayed in Fig. 4a. From the peak positions, we can unambiguously deduce that the purchased powder is α-PVDF, in agreement with literature.

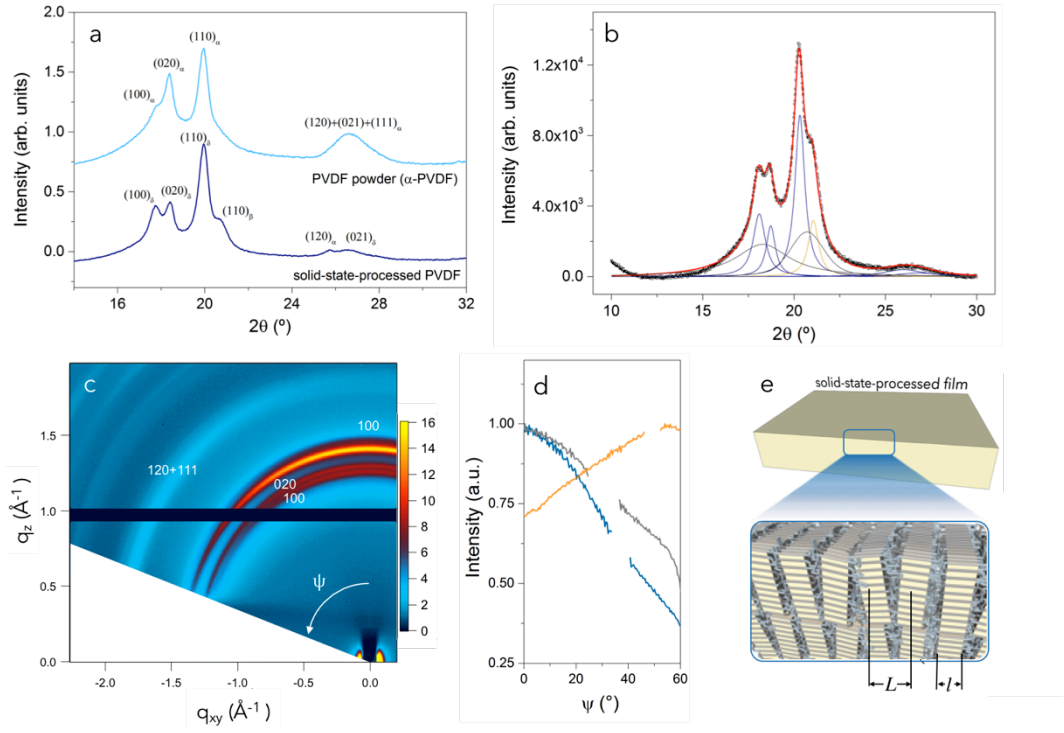

Fig. 4. X-ray diffraction data of solid-state-processed PVDF films. (a) WAXS θ-2θ scans of solid-state-processed PVDF (dark blue line) and commercially bought PVDF powder (*i.e.*, α-PVDF; light blue line). (b) Decomposition of the WAXS θ-2θ scans into elementary peaks of the δ-, α-, and β-phases. Relevant diffractions of the δ- and α-phase are plotted in blue, those of the β-phase are shown in orange and contribution of the amorphous halo in grey. The broad peaks correspond to the contribution of the amorphous halo. (c) 2D-WAXS pattern of solid-state processed PVDF films (*z* corresponds to the direction normal to the film *x*-*y* plane). (d) WAXS intensity of the (110) reflection (blue line), ((100) + (020)) reflections (grey line) and ((120) + (021)) reflections (orange line) plotted against the ψ-angle, which is the angle defined by the rotation of the sample around an axis contained in the plane of the film (*x*-*y* plane). (e) Schematic illustration of the preferential crystal orientation that we deduce from our X-ray data presented in a,b for solid-state-processed films.

Since (i) both samples (as-received powder and solid-state pressed film) feature identical X-ray diffraction patterns (Fig. 4a and Fig. S2 of the ESI†), (ii) it is known that the polar δ-PVDF features the same crystal structure as the non-polar α-phase, and (iii) the solid-state pressed films are piezoelectric, we further conclude that the solid-state pressed sample is comprised of the δ-phase.

The similarity in the X-ray diffraction pattern of the δ-phase with α-PVDF renders, however, full identification of the δ-phase by X-ray diffraction challenging[19]. Some conclusions can nonetheless be drawn. For instance, the shoulder at ~21° that we observe for the solid-state pressed films indicates that a small amount of β-PVDF is present in our solid-state pressed films. We like to note, though, that when deconvoluting these WAXS pattern into the contributions of the α, β and δ phases (Fig. 4b), we deduce that the amount of β-phase in the films is less than ~10 %, which is far too small to dominate their piezoelectric behaviour.

We also conducted 2D-WAXS experiments to gain further insights into solid-state processed PVDF films (experimental conditions are shown in ESI†). Fig. 4c shows the diffracted WAXS intensity (in colour scale) of solid-state pressed films, plotted against q_z and q_{xy}, *i.e.* the wave vectors normal and parallel to the plane of the film. Arch-like diffractions were recorded for all Bragg maxima indicating a continuous distribution of crystal orientations within these films. The distribution can be obtained from the intensity profiles of the diffraction maxima along the ψ-angle, that is the angle defined by the rotation of the sample around an axis contained in the plane of the film (*x*-*y* plane). Fig. 4d shows that the intensity of (110) and (100+020) reflections decrease when approaching the equator, while that of the (021) reflection increases. These tendencies are indicative of a preferred crystal orientation where the *c*-axis (*i.e.* the direction of along the chains) of this PVDF polymorph points parallel

to the plane of the film, as schematically depicted in Fig. 4e (see also Supporting Information Fig. S3), similar to what was reported for poly(3-hexylthiophene) (P3HT) when it was processed via solid-state pressing [24].

Additional information was obtained from estimating the lamellar crystal thickness, *l*, of the ordered moieties present in solid-state pressed structures, using for this purpose small-angle X-ray scattering and differential scanning calorimetry (DSC) data (see ESI† Fig. S4). We have indicated *l* in the schematic of the solid-state processed structure displayed in Fig. 4e. Both solid-state-processed PVDF and α-PVDF films, produced from solution, feature well-defined Bragg peaks in the low *q*-region of the respective SAXS profiles (ESI† Fig. S4b). The peak for the solid-state pressed PVDF is centred at $q \sim 0.049$ Å^{-1}, which corresponds to a characteristic length of the periodic stack, *i.e.* the so called long period *L*, which is comprised of the thickness of the crystalline lamella as well as the one of the unordered fraction in this stack (see also Fig. 4e). We find that $L \approx 12.8$ nm for solid-state pressed films, while for α-PVDF (processed from solution), a long period $L \approx 12.1$ nm is extracted.

Since the lamellar crystal thickness can be calculated from $l = L \cdot X$ where *X* is the degree of crystallinity, we can deduce *l* when estimating *X* from thermal analysis data. Both, α-and solid-state pressed PVDF display similar thermograms with a single dominant endotherm that is associated with the melting of the crystalline fraction in these structures (ESI† Fig. S4a). Assuming that both phases possess equal values for the enthalpy of fusion, ΔH_f, for a 100% crystalline material of 104.5 J/g [26], we estimate *X* to be 42% for solid-state pressed PVDF and 44% for α-PVDF. Clearly, and despite the high weight-average molecular weight of the PVDF used here (543 kg/mol), the degree of crystallinity does not change with solid-state-processing. The lamellar crystal thickness, *l*, is also similar in both cases and is calculated to be 5.4 nm.

The mechanism of the transition of α-PVDF into δ-PVDF remains unclear. The driving force for the change of molecular orientation upon high-field poling is probably the applied electric field, which induces the re-orientation of the normal component of the dipole moment of specific chain segments and, in turn, leads to the chain segments' physical rotation [27, 28, 29]

However, in solid-state processing no electric field is applied; hence, the antiparallel-to-parallel chain reorientation that is required to induce a transition from the α- to the δ-polymorph, must have a different origin. We propose here that at the temperatures and pressures used during solid-state-processing, the δ-PVDF may be the thermodynamically stable phase. The physical rotation of chain segments needed for the α- to δ-phase transition to occur, might, thereby, be assisted by the dynamics of the PVDF chain segments within the α-crystals. Indeed, while the PVDF macromolecules in the α-polymorph are fully frozen at room temperature [30], a local dynamic process, commonly referred to the as the α_c relaxation, starts to be operative above 100-120 °C [9, 30] — *i.e.* in the temperature range where solid-state pressing started to result in fully compact and optically transparent films. The precise molecular motion leading to this α_c relaxation is not fully understood; however, it is generally accepted that it originates from rotational or conformational motions along the PVDF chains [30, 31, 32]. Hence, in the case of solid-state processing PVDF, certain bonds and atoms along this polymer's chains can exhibit rotational dynamics in the temperature regime where the α_c relaxation sets in. These rotations may facilitate the transition from an antiparallel-to-parallel orientation of the PVDF chains and, as a consequence, the phase transition from the α- to δ-polymorph. This hypothesis is supported by the fact that we were not able to fabricate coherent films in the solid state at temperatures below the α_c-relaxation temperature.

Note, finally, that it was previously suggested that a transition from δ-PVDF to the less polar γ-phase may occur at temperatures slightly below the melting of these PVDF phases [33]. This would lead to a reduction in the piezoelectric performance of the free-standing films. We, therefore, assessed the thermal behavior of solid-state pressed PVDF films with differential scanning calorimetry (Supporting Information Fig. S4a). Independent of the heating rate used, the melting endotherm is the only noticeable feature we observed for solid-state pressed material in the temperature range analyzed. This suggests that no solid-solid phase transition occurs in such PVDF structures. This finding is important from a technological point of view, because a potential transition into a less polar phase

would be accompanied by loss of remanent polarization and a decrease of the piezoelectric charge coefficient.

Conclusions

In summary, we have demonstrated a one-step process that is commonly used to produce PTFE items without affecting this polymer's properties, can be exploited to realise piezoelectric and ferroelectric PVDF structures. The advantage of this processing route is that straight-forward compression molding under moderate pressures and temperatures suffice to apparently lead to a solid-state transition from the technologically relatively uninteresting apolar α-PVDF (commercially available as powder) to the fully piezoelectric δ-phase. Indeed, standard manual laboratory hot presses can be used for this process. The transition from the apolar to polar phase may result from a higher thermodynamic stability of the δ-phase under those conditions; it may also be assisted by the dynamics of the chain-segments within α- PVDF, *i.e.* the α_c relaxation. The coercive field for the saturated ferroelectric loop for such solid-state pressed PVDF films is 110 MV/m, while the saturated polarization is 7 μC cm^{-2}. The piezoelectric charge coefficient is -36 pm/V. Intriguingly, this value is comparable to that of biaxially stretched β-PVDF (-31 pm/V); and it is notably higher than values previously reported for electroformed δ-PVDF (-31 resp. -15 pm/V). The structural analysis of solid-state pressed PVDF reveals a partial orientation of the polymer chains in plane of the films, which likely is due to the compression forces that act during solid-state pressing. The degree of crystallinity of such structures can be deduced to be ~42%, while the lamellar thickness *l* was estimated to be 5.4 nm, with the long period *L* extracted as 12.8 nm. Since these values are similar to those obtained for α-PVDF, we conclude that solid-state-processing does not induce strong changes in the internal structure of the material other than the phase transformation to the δ-PVDF. Most importantly, the simplicity of solid-state processing to induce a polar, fully piezoelectric form of PVDF, allowing to shape the polymer in various structures, and the increased thermal stability of the PVDF homopolymer compared to its copolymers [19, 34] may open a range of new possibilities for this interesting material not only for further fundamental studies but also for future industrial production of piezoelectric plastic films.

Author contributions

N.S., D.M.d.L. and I.K. conceived the idea. J.M. prepared the solid-state processed films and performed the structural and thermal characterization and analyzed the data. T.L. and D.Z fabricated the spin-cast films and conducted the electrical characterization for all samples. D.Z. and I.K. analyzed the electrical results. J.M., D.Z., T.L., I.K., D.M.d.L., and N.S. co-wrote and commented on the manuscript. D.M.d.L. and N.S. supervised the project.

Acknowledgements

J.M. acknowledges support from the European Union's Horizon 2020 research and innovation programme under the Marie Skłodowska-Curie grant, agreement No 654682. T. L. acknowledges financial support by the Graduate School Materials Science in Mainz. N.S. is in addition grateful for support by a European Research Council ERC Starting Independent Research Fellowship under the grant agreement No. 279587. We further acknowledge A. Arbe and A. Iturrospe for their invaluable assistance with SAXS measurements, and L. Yu, R. Li and D.-M. Smilgies for 2D-WAXS experiments at CHESS.

References

1. H. Kawai, *Jpn. J. Appl. Phys*, 1969, **8**, 975.
2. I. Katsouras, K. Asadi, M. Li, T. B. van Driel, K. S. Kjaer, D. Zhao, T. Lenz, Y. Gu, P. W. M. Blom, D. Damjanovic, M. M. Nielsen and D. M. de Leeuw, *Nat. Mater.*, 2016, **15**, 78-84.
3. M. Zirkl, A. Sawatdee, U. Helbig, M. Krause, G. Scheipl, E. Kraker, P. A. Ersman, D. Nilsson, D. Platt, P. Bodö, S. Bauer, G. Domann and B. Stadlober, *Adv. Mater.*, 2011, **23**, 2069-2074.
4. Z. Hu, M. Tian, B. Nysten and A. M. Jonas, *Nat. Mater.*, 2009, **8**, 62-67.
5. K. Fukuda, T. Sekitani, U. Zschieschang, H. Klauk, K. Kuribara, T. Yokota, T. Sugino, K. Asaka, M. Ikeda, H. Kuwabara, T. Yamamoto, K. Takimiya, T. Fukushima, T. Aida, M. Takamiya, T. Sakurai and T. Someya, *Adv. Funct. Mater.*, 2011, **21**, 4019-4027.
6. B. Jadidian, N. M. Hagh, A. A. Winder and A. Safari, *IEEE Trans. Sonics Ultrason.*, 2009, **56**.
7. D. Zhao, I. Katsouras, K. Asadi, W. A. Groen, P. W. M. Blom and D. M. de Leeuw, *Appl. Phys. Lett.*, 2016, **108**.
8. A. J. Lovinger, *Science*, 1983, **220**, 1115-1121.

9. A. J. Lovinger, in *Developments in Crystalline Polymers—1*, ed. D. C. Bassett, Springer Netherlands, Dordrecht, 1982, DOI: 10.1007/978-94-009-7343-5_5, pp. 195-273.
10. M. A. Bachmann and J. B. Lando, *Macromolecules*, 1981, **14**, 40-46.
11. J. B. Lando, H. G. Olf and A. Peterlin, *J. Polym. Sci. A-1: Polym. Chem*, 1966, **4**, 941-951.
12. Y. L. Gal´perin, Y. V. Strogalin and M. P. Mlenik, *Vysokomol. Soed.,* 1965, **7**, 933.
13. P. Martins, A. C. Lopes and S. Lanceros-Mendez, *Prog. Polym. Sci.*, 2014, **39**, 683-706.
14. A. J. Lovinger, *Macromolecules*, 1982, **15**, 40-44.
15. M. Bachmann, W. L. Gordon, S. Weinhold and J. B. Lando, *J. Appl. Phys.*, 1980, **51**, 5095-5099.
16. G. T. Davis, J. E. McKinney, M. G. Broadhurst and S. C. Roth, *J.Appl. Phys.*, 1978, **49**.
17. G. T. Davis and H. Singh, *Polymer*, 1979, **20**.
18. D. Naegele, D. Y. Yoon and M. G. Broadhurst, *Macromolecules*, 1978, **11**, 1297-1298.
19. M. Li, H. J. Wondergem, M.-J. Spijkman, K. Asadi, I. Katsouras, P. W. M. Blom and D. M. de Leeuw, *Nat. Mater.*, 2013, **12**, 433-438.
20. M.-C. Garcia-Gutierrez, A. Linares, J. J. Hernandez, D. R. Rueda, T. A. Ezquerra, P. Poza and R. J. Davies, *Nano Lett*, 2010, **10**, 1472-1476.
21. S. J. Kang, I. Bae, J.-H. Choi, Y. J. Park, P. S. Jo, Y. Kim, K. J. Kim, J.-M. Myoung, E. Kim and C. Park, *J. Mater. Chem.*, 2011, **21**, 3619-3624.
22. H. Ohigashi, *J. Appl. Phys.*, 1976, **47**, 949-955.
23. S. Ebnesajjad, *Fluoroplastics volume 1: Non-Melt Processible Fluoroplastics*, 2000.
24. M. A. Baklar, F. Koch, A. Kumar, E. B. Domingo, M. Campoy-Quiles, K. Feldman, L. Yu, P. Wobkenberg, J. Ball, R. M. Wilson, I. McCulloch, T. Kreouzis, M. Heeney, T. Anthopoulos, P. Smith and N. Stingelin, *Adv. Mater.*, 2010, **22**, 3942-3947.
25. Collison D. *Methods in Rock Magnetism and Palaeomagnetism: Techniques and Instrumentation* Springer: The Netherlands, 2013.
26. K. Nakagawa and Y. Ishida, *J. Polym. Sci.: Polym. Phys. Ed.*, 1973, **11**, 2153-2171.
27. H. Dvey-Aharon, P. L. Taylor and H. A. J., *J. Appl. Phys.*, 1980, **51**.
28. A. J. Lovinger, *Macromolecules*, 1981, **14**, 225-227.
29. W. Wang, H. Fan and Y. Ye, *Polymer*, 2010, **51**, 3575-3581.
30. H. Sasabe, S. Saito, M. Asahina and H. Kakutani, *J. Polym. Sci. . A-2: Polym. Phys.*, 1969, **7**, 1405-1414.
31. Y. Miyamoto, H. Miyaji and K. Asai, *J. Polym. Sci.: Polym. Phys. Ed.*, 1980, **18**, 597-606.
32. Y. Miyamoto, *Polymer*, 1984, **25**.
33. B. Servet and J. Rault, *J. Phys. France*, 1979, **40**, 1145-11.
34. M. Li, N. Stingelin, J. J. Michels, M.-J. Spijkman, K. Asadi, K. Feldman, P. W. M. Blom and D. M. de Leeuw, *Macromolecules*, 2012, **45**, 7477-7485.